Applied Surface Science 659 (2024) 159876

Contents lists available at ScienceDirect

Applied Surface Science

journal homepage: www.elsevier.com/locate/apsusc

Full Length Article

Using sputtering parameters to mitigate argon ion sputtering induced reduction of nickel in XPS

Craig Moore, Jeremy Moon, Dev Chidambaram *

Chemical and Materials Engineering, University of Nevada, Reno – 1664 N. Virginia St., Reno, NV 89557-0388 United States

ARTICLE INFO

Keywords:
Sputtering Reduction
XPS
Nickel Oxide
Cluster argon ion sputtering

ABSTRACT

Argon ion sputtering for depth profiling in XPS results in the preferential sputtering of oxygen in certain oxide systems. Preferential oxygen removal results in the chemical reduction of the associated cation which is observed in spectra collected following sputtering. Characterizing the effects of different sputtering parameters and developing methods to account for and to minimize changes to chemical states during sputtering would allow for greater confidence in the qualitative and quantitative analysis of the chemical states observed after sputtering. In this study argon ion sputtering was performed with monatomic and clustered argon ions on thermally oxidized NiO. Parameters for monatomic and cluster sputtering were varied to observe their effects on the induced reduction. Results show that extensive reduction is experienced for monatomic sputtering irrespective of the energy and current chosen. For cluster argon ion sputtering, reduction was mitigated when selecting either large cluster sizes or low cluster energies. Sputtering for long periods of time with low energy clusters was observed to result in the removal of surface contaminants without concomitant reduction of the nickel oxide.

1. Introduction

X-ray photoelectron spectroscopy (XPS) is a commonly used technique to investigate the elemental composition and chemical state of surfaces. Determination of the chemistry of surfaces provides useful information for multiple fields of research including corrosion science, catalysts, semiconductors, and many others [1]. Due to the sensitivity (~0.2 at% detection limit) and shallow sampling depth (within ~ 10 nm) of XPS, sputtering of the surface may be required either to clean the surface from unwanted contaminants or to etch the sample surface, allowing for underlying material to be analyzed. Sputtering in XPS is accomplished through surface bombardment with ionized gas with monatomic argon ions and clustered argon ions being the most prevalent [2,3]. Ideally, these ions remove sample material evenly with respect to sample chemistry. However, a frequently observed artifact of sputtering in oxygen bearing materials is the reduction of select cations due to the preferential sputtering of oxygen [4,5]. Multiple studies have observed that oxides following sputtering have oxidation states reduced relative to their un-sputtered state [5,6]. Preferential sputtering in multi component systems can be attributed to multiple phenomena [7,8]. It has been suggested that mass differences between atoms in a material results in preferential loss of the lighter component which has been observed for select oxides and binary alloys due to uneven energy and momentum propagation [7]. However, mass differences alone are not enough to describe preferential sputtering as other alloy systems have experienced preferential sputtering of the heavier component [8]. This can be accounted for by also considering the chemical binding energy at the surface where is has been shown that components that form weaker bonds are removed preferentially [8]. A component of chemical bonding effects are thermal effects which arise from localized thermal spikes at the location of argon impact which may result in the decomposition of the target [8]. Reduction characteristics vary depending on the sputtering parameters, which dictate the energy the incident ions deliver to the sample surface. Recently, clustered argon ion sputtering systems have been developed and made commercially available. These systems aim to etch samples more “gently” relative to monatomic argon ion sources to minimize selective oxygen sputtering and other unwanted effects. Compared to monatomic argon ion sputtering, clustered argon ion sputtering to equivalent depths has shown to cause a lower degree in reduction for Ta_2O_5 and TiO_2 [9,10]. Although cluster argon ion sputtering reduces the severity of the observed reduction, it has not been shown to eliminate the experienced reduction.

The use of argon ion sputtering for depth profiling with XPS is desirable in corrosion science as oxide films and underlying metal

* Corresponding author.
E-mail addresses: craigmoore@nevada.unr.edu (C. Moore), jeremymoon@unr.edu (J. Moon), dcc@unr.edu (D. Chidambaram).

https://doi.org/10.1016/j.apsusc.2024.159876
Received 10 November 2023; Received in revised form 4 March 2024; Accepted 9 March 2024
Available online 11 March 2024

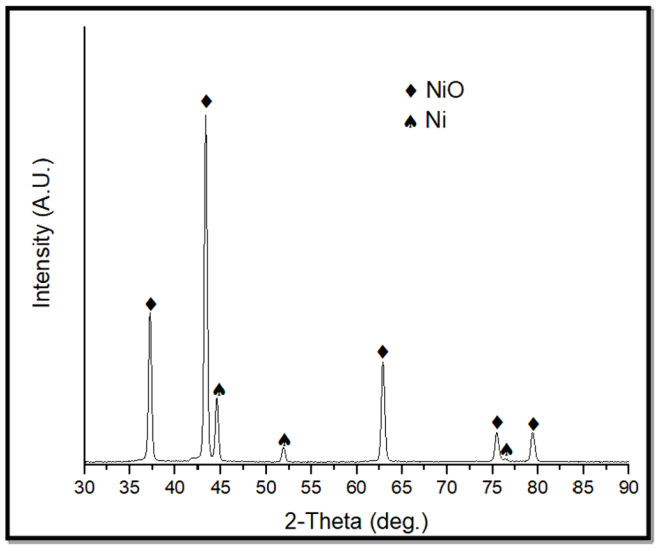

Fig. 1. X-ray diffraction pattern for thermally oxidized nickel metal. NiO and Ni were identified from the diffraction pattern.

compositions are often inhomogeneous with respect to depth after exposure to corrosive environments, and XPS depth profiling can provide vital information about the composition and chemistry of the surface and near surface regions [11–14]. In nickel bearing transition metal samples, our group has shown that sputtering with monatomic argon preferentially reduces oxidized nickel while other elements such as iron and chromium remain unaffected [15]. Nickel is an important alloying element for industrial alloys used in structural and container applications (e.g., Alloy 600, Alloy C-276, austenitic steels like SS316, etc) and it is typically present in the oxide layers of these alloys after exposure to corrosive environments [16–18]. Accurately detecting its chemical state throughout the depth of the oxide and underlying metal layers is important for understanding corrosion in these alloys. While knowledge of sputtering induced reduction can allow the observed reduction to be accounted for, it would be ideal to avoid sputtering induced chemical damage to increase confidence in the assignment and quantification of observed chemical states. In this study, nickel metal was thermally oxidized to form NiO and subsequently sputtered with both monatomic and clustered argon ions. Sputtering parameters including cluster size and acceleration voltage were varied systematically to explore their effects on sputtering induced reduction.

2. Material and methods

2.1. Sample Preparation

A sheet of Nickel 200 (McMaster-Carr, >98 % pure) was obtained and subsequently cleaned through ultrasonication in isopropanol. The surface of the cleaned nickel 200 was oxidized by thermal oxidation at 800 ℃ in a laboratory box furnace under ambient atmosphere for 72 h.

2.2. X-ray diffraction

Grazing incidence X-ray diffraction (XRD) patterns were obtained with a Rigaku Smartlab X-ray diffractometer with a Cu K α X-ray source operating at 44 kV and 40 mA using parallel beam optics and an X-ray incidence angle of 1°.

2.3. Scanning electron microscopy

Scanning electron microscopy (SEM) imaging, X-ray energy dispersive spectroscopy (EDS), and focused ion beam (FIB) milling were carried out using a ThermoFisher Scios2 dual-beam SEM/FIB with a TEAM Pegasus Integrated EDS. The electron beam was operated at 20 kV and 1.6nA for imaging and EDS analysis. For FIB milling, a ~ 3 μm thick layer of Pt was deposited on the sample surface over the area of interest

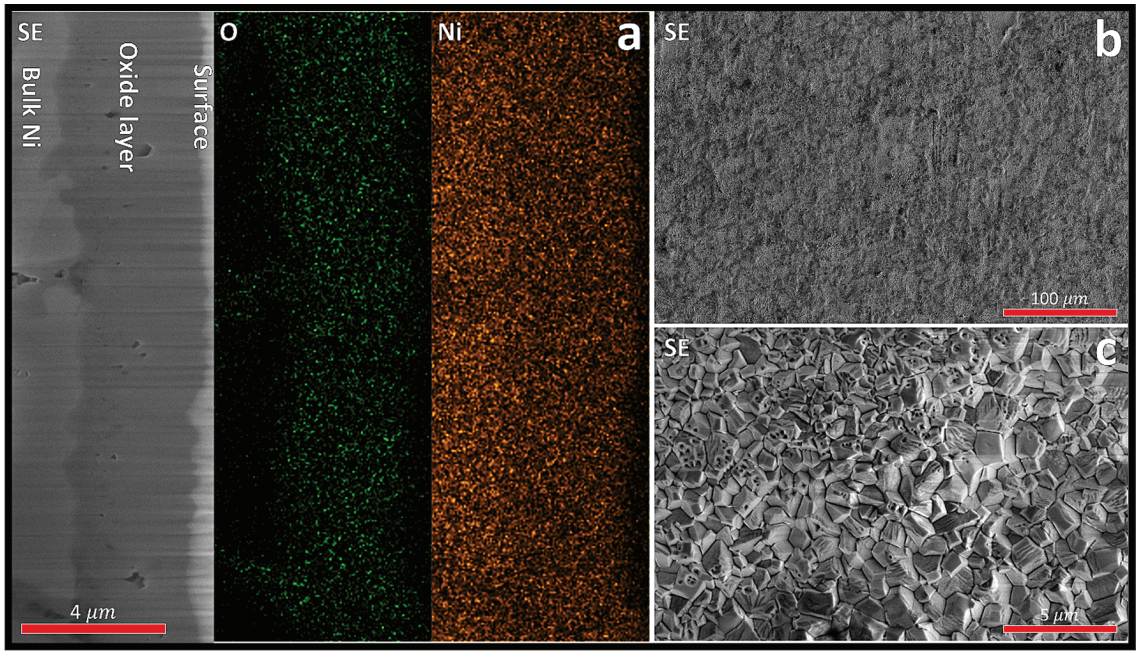

Fig. 2. (a) SEM secondary electron image of a FIB-milled cross section of the oxidized nickel plate. The oxide layer is the dark region to the right side of the image and the bulk nickel metal is the lighter region to the left side of the image. The thin, very light layer visible on the extreme right edge is a layer of platinum deposited using ion beam induced deposition to protect the sample surface during ion beam milling. The oxide layer is ~ 4 μm thick. The EDS maps of oxygen and nickel show that oxygen is concentrated in the dark layer and the concentration of nickel is slightly depleted relative to the bulk due to the presence of oxygen. The surface oxide morphology is shown in (b) at low magnification and (c) at high magnification. The oxide layer is thick relative to the depth of argon ion sputtering used in this work (4 μm oxide vs. ~ 10 nm sputtering depth) and all nickel metal observed in the Ni 2p spectra can be attributed to argon ion induced effects.

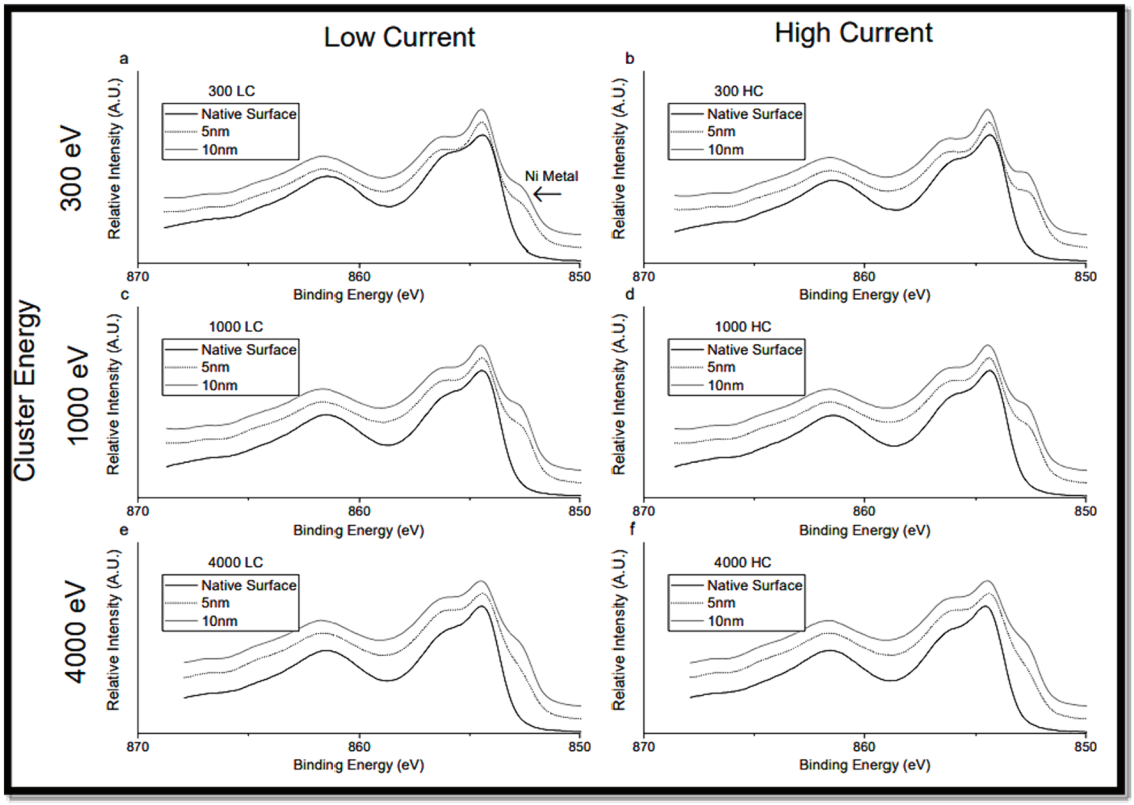

Fig. 3. Oxidized nickel metal spectra recorded before and after two stages of monatomic depth profiling. Two sputtering steps at an estimated depth of 5 nm per step based on the theoretical sputtering rate of Ta_2O_5 were performed at different energies and current settings.

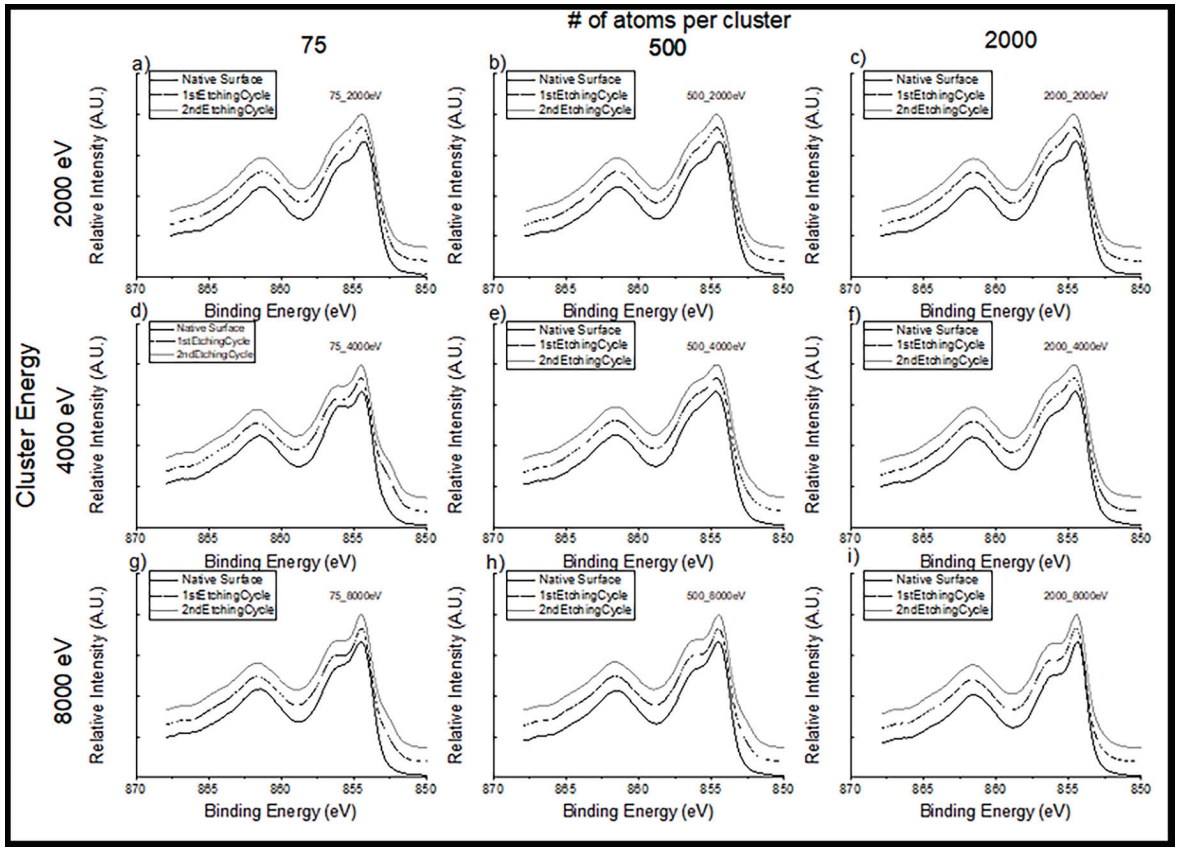

Fig. 4. Oxidized nickel sputtering with varied cluster sputtering settings indicated at the beginning of rows and columns. For 2000 eV, 4000 eV, and 8000 eV cluster sputtering steps, the sample was sputtered for 600 s, 300 s and 100 s respectively.

using ion beam assisted deposition with a 30 kV, 1nA beam. The cross section was then milled perpendicular to the sample surface using Ga ions with a 30 kV, 50nA ion beam for initial material removal. Subsequent milling at 30 kV with 7.5nA and then 3nA ion beam currents was carried out to produce a smooth cross-sectional surface.

2.4. X-ray photoelectron spectroscopy

XPS studies were performed using a ThermoFisher Scientific Nexsa G2 Surface Analysis System with a monochromatic Al X-ray source ($h\nu$ = 1486.6 eV) operated at 12 kV and 10 mA with a spot size of 400 μm. Recorded spectra were collected with a pass energy of 50 eV. The instrument was calibrated to the Au $4f_{7/2}$ metallic binding energy (BE) at 84.1 eV. Recorded spectra were peak fit using Thermo Fisher Scientific Avantage software.

The Nexsa G2 integrated Monatomic and Gas Cluster Ion Source (MAGCIS) dual beam ion source was used for sputtering of the sample surface. Sputtering areas were set to 2 mm x 2 mm and each individual sputtering location was moved 3 mm from adjacent location to ensure that individual sputtering experiments did not overlap. The pressure of the instrument during ion-beam etching was 2 X 10^{-7} mBar.

Monatomic argon ions at energies of 300, 1000 and 4000 eV and two current levels, low current (LC) and high current (HC), were used for sputtering. The high current mode has a sputtering rate approximately three times that achieved with low current, but the instrument manufacturer does not specify the ion flux for these modes. A total of 10 nm (Ta_2O_5 equivalent) was etched in two etching cycles of 5 nm (Ta_2O_5 equivalent) each.

Cluster argon sputtering was completed with three energy levels (2000 eV, 4000 eV, 8000 eV) and three different cluster sizes (75atoms, 500 atoms, 2000 atoms). Since the sputtering rate vs. time relationship for the cluster argon source is currently unknown, etching times of 600 s, 300 s and 100 s were selected for energies of 2000 eV, 4000 eV, and 8000 eV, respectively, and two etching cycles were carried out. Due to the low etching rate achieved through cluster sputtering, it is unlikely that 10 nm of etching was performed and thus the cluster sputtering results may not be directly comparable to the monoatomic sputtering. Monatomic argon ions of 4000 eV was used to sputter through the native oxide of a separate, non-thermally oxidized, nickel 200 sample in order to collect nickel metal spectra. Based on the results from the cluster sputtering, long term sputtering cycles were performed with 4000 eV 500 atom clusters and 2000 eV 75 atom clusters for three etching cycles of one hour and two hours per cycle respectively.

Peaks fit to the recorded spectra of Ni metal and native NiO were used as a reference to fit the metal and NiO components present in the collected spectra. Nickel metal and NiO were fit with three and five peaks respectively, as proposed by Biesinger *et al.* [19]. Peak positions and full width at half maxes (FWHM) were allowed to vary by 0.1 eV to account for statistical deviations present in the collected spectra. Peak height ratios were kept constant. Spectra collected from the native surface were charge corrected to the C1s peak of adventitious carbon at 284.8 eV. Sputtered spectra were shifted to the first peak of oxidized nickel found from the initial charge correction. Notably, the use of adventitious carbon has been criticized recently due to a lack of repeatability. The variability in reported binding energies has been a result of inconsistent charge correction and thus different methods may need to be used if the species of interest are unknown [20]. For this study, charge correction using adventitious carbon was found to be consistent throughout the performed experiments as observed from other spectra (such as NiO) as well. Additionally, it should be emphasized here that the charge correction for carbon itself does not affect the results of the study which is focused on reduction of nickel oxide to nickel metal which have distinct spectral features.

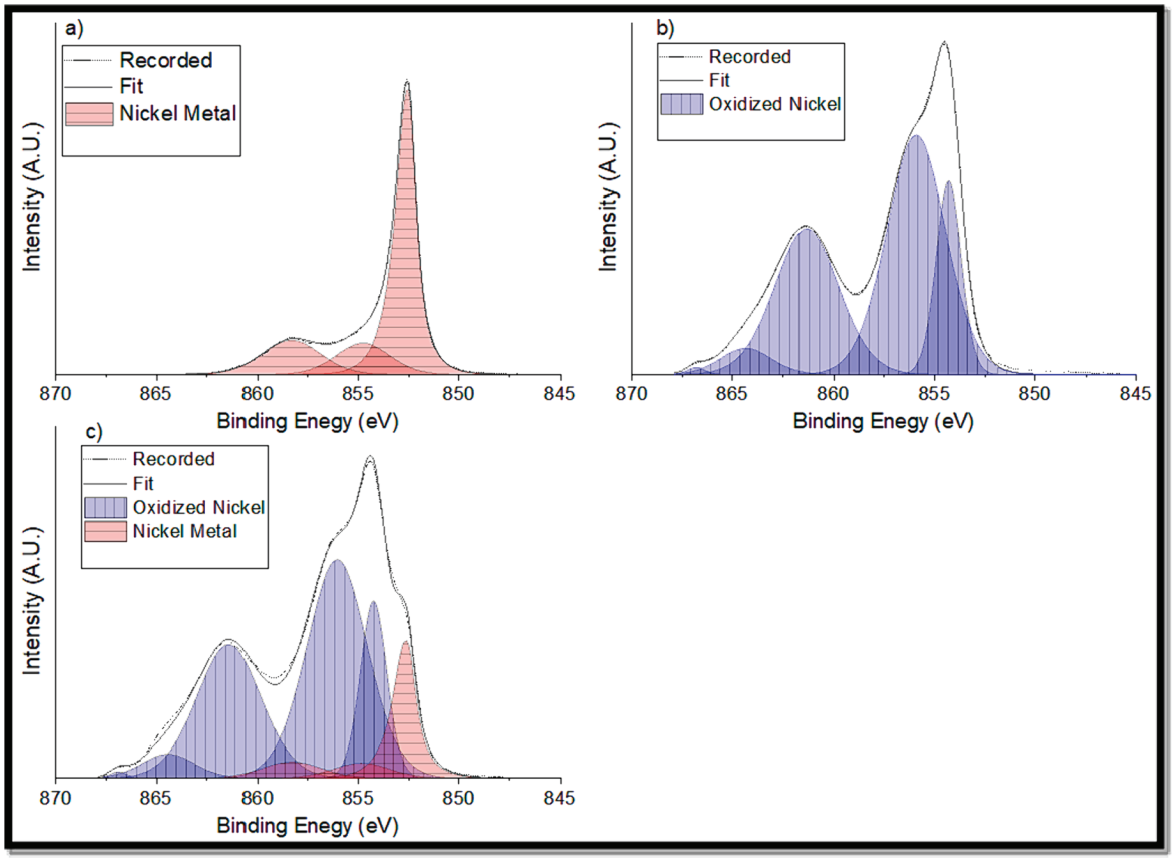

Fig. 5. a) nickel metal spectra, b) native oxidized nickel metal, c) oxidized nickel metal sputtered with 4000 eV monatomic argon ions.

3. Results and discussion

3.1. Oxide layer characterization

Fig. 1 contains the X-ray diffraction pattern for the oxidized nickel metal. The pattern obtained from the thermally oxidized sample contains peaks corresponding to NiO and Ni (JCPDF 00–047-1049 and 00–004-0850, respectively). Although the base nickel metal is present in the recorded pattern, it is unlikely that it is contributing signal to the XPS spectra as the penetration depth of XRD is on the order of hundreds of nanometers to microns and the NiO that is formed is on the surface. Due to the shallow interaction depth of XPS (~10 nm), the nickel metal signal recorded with XPS originates entirely from oxidized nickel that has been reduced through sputtering.

To confirm that XPS depth profiling and chemical state analysis were only accessing the thermally oxidized nickel layer and not the base nickel metal, FIB etching and EDS composition analysis were performed to determine the thickness of the thermally oxidized nickel layer. Fig. 2a shows secondary electron micrographs of a focused ion beam (FIB) milled cross section of the oxidized Ni sample. EDS mapping, shown in Fig. 2a, indicates that the dark layer extending into the sample from the sample surface contains oxygen, confirming that it is the thermally grown oxide layer. This layer is ~ 4 μm thick. The maximum estimated depth of argon ion sputtering is on the order of tens of nanometers into the sample and no breakthrough of the oxide layer is anticipated, so any metallic Ni signal observed in the Ni 2p XPS spectra can be confidently attributed to chemical shifts related to argon ion sputtering. The surface morphology of the oxide layer is homogenous across the sample surface, as shown in Fig. 2b and 2c and EDS analysis of the surface shows that the surface is composed of Ni and O in a roughly 1:1 ratio, corresponding to the NiO phase observed using XRD.

3.2. Monatomic argon sputtering

Fig. 3 shows the Ni $2p_{3/2}$ photoelectron spectra for the thermally oxidized nickel sputtered with monatomic argon ions. The shoulder assigned as nickel metal at 852.6 eV is present in spectra obtained using monatomic ions at all energy and current combinations and increases with increasing sputtering time and depth. All monatomic sputtering parameters produced a significant amount of intensity in the region associated with nickel metal that can be attributed to the sputtering-induced reduction of NiO to nickel metal.

3.3. Cluster argon sputtering

Fig. 4 contains the Ni $2p_{3/2}$ spectra for nickel oxide sputtered with clustered argon ions. As shown in Fig. 4d, 4e, 4 g, and 4 h, sputtering induced reduction is present for 8000 eV and 4000 eV energies with cluster sizes of 75 ions and 500 ions. For these higher energies, reduction is significantly reduced at higher cluster sizes, as shown in Fig. 3f and 3i. Notably, it has been shown that decreased energy (E) to cluster size (n) ratios result in decreased sputtering yields [21], which may correlate to a lower sputtering rate, resulting in the reduced amount of metal nickel found when larger clusters were used. Although the E/n ratio influences the observed reduction characteristics as indicated by the higher energy cluster sputtering experiments, it is not sufficient to fully determine the extent of reduction. When sputtering at an energy of 2000 eV, extensive reduction was avoided irrespective of the cluster size employed. The E/n ratio was 26.67 eV/atom at cluster sizes of 75 atoms for the 2000 eV energy. Considering that a greater extent of sputtering reduction is observed using a cluster energy of 4000 eV and size of 500 atoms (8 eV/atom), the reduced amount of observed reduction at a higher E/n value of 26.67 indicates that the sputtering characteristics are not just determined by E/n as proposed by Seah, [21] but also by the total cluster energy. Notably, it has been shown that low energy clusters may not be able to remove metallic oxide material from the sample [22] and thus

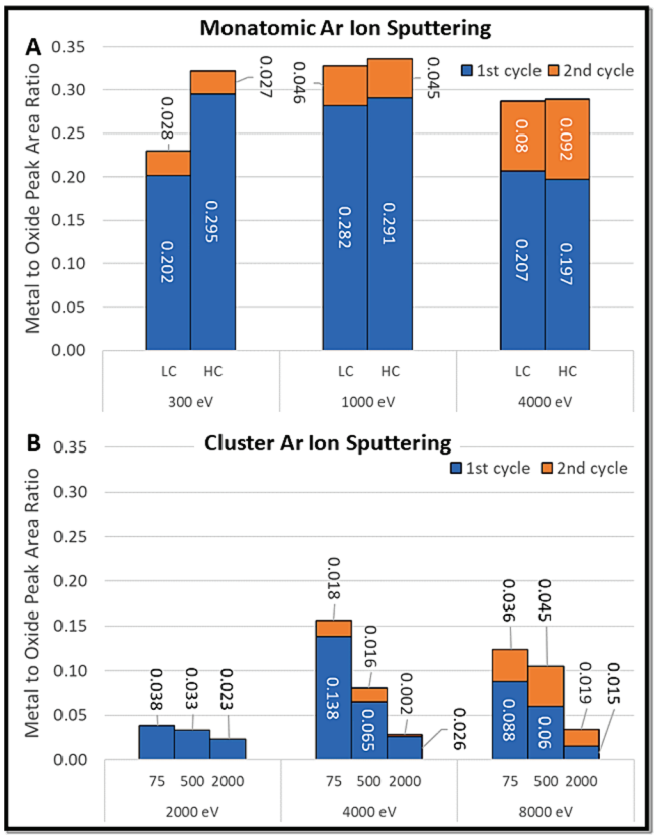

Fig. 6. Metal to oxide peak area ratios for oxidized nickel sputtered with (A) monatomic argon ions at different energy for the low current (LC) and high current (HC) setting and (B) cluster argon ions at different cluster energy and sizes. The annotation for the first sputtering cycle shows the metal to oxide peak area ratio generated in that round of sputtering, while the annotation for the second sputtering cycle indicates the change in metal to oxide peak area generated in that sputtering cycle.

the lack of reduction may be attributable to a lack of sputtering of the NiO. While active removal of the NiO is desirable, the ability of the low energy clusters to sputter the adsorbed organic layer without altering the chemical state of the oxide is useful in its own regards.

3.4. Quantitative reduction comparison

Fig. 5a and 5b show the peak fits used for nickel metal and the native oxidized nickel respectively. Fig. 5c contains the spectra collected from the oxidized nickel after sputtering with the monatomic source at 4000 eV to a depth of 10 nm (Ta_2O_5 equivalent). Inconsistencies between the fit and collected spectra following sputtering may be attributed to the potential presence of $Ni(OH)_2$ that may exist on the surface due to exposure of the sample to air at ambient temperature following heat treatment [23]. Since the distribution of reduced nickel produced by sputtering is unknown, estimation of the true atomic percentages of oxide and metal was not performed as the depth distribution function for this system is not known. Comparing the relative peak areas between the metal and the oxide gives a semiquantitative extent of reduction, allowing the different sputtering parameters to be compared.

Fig. 6 shows the area ratios of the primary metal peak at 852.6 eV over that of the largest oxide peak at 855.9 eV. For all monatomic sputtering parameters, the ratio of metal to oxide increases with additional sputtering, as shown by the increase in metal to oxide from the first 5 nm sputtering cycle to the second 5 nm cycle (Fig. 6a). Between the sputtering parameters, a lower extent of reduction was observed for the highest energy 4000 eV argon ions as well as the low current 300 eV

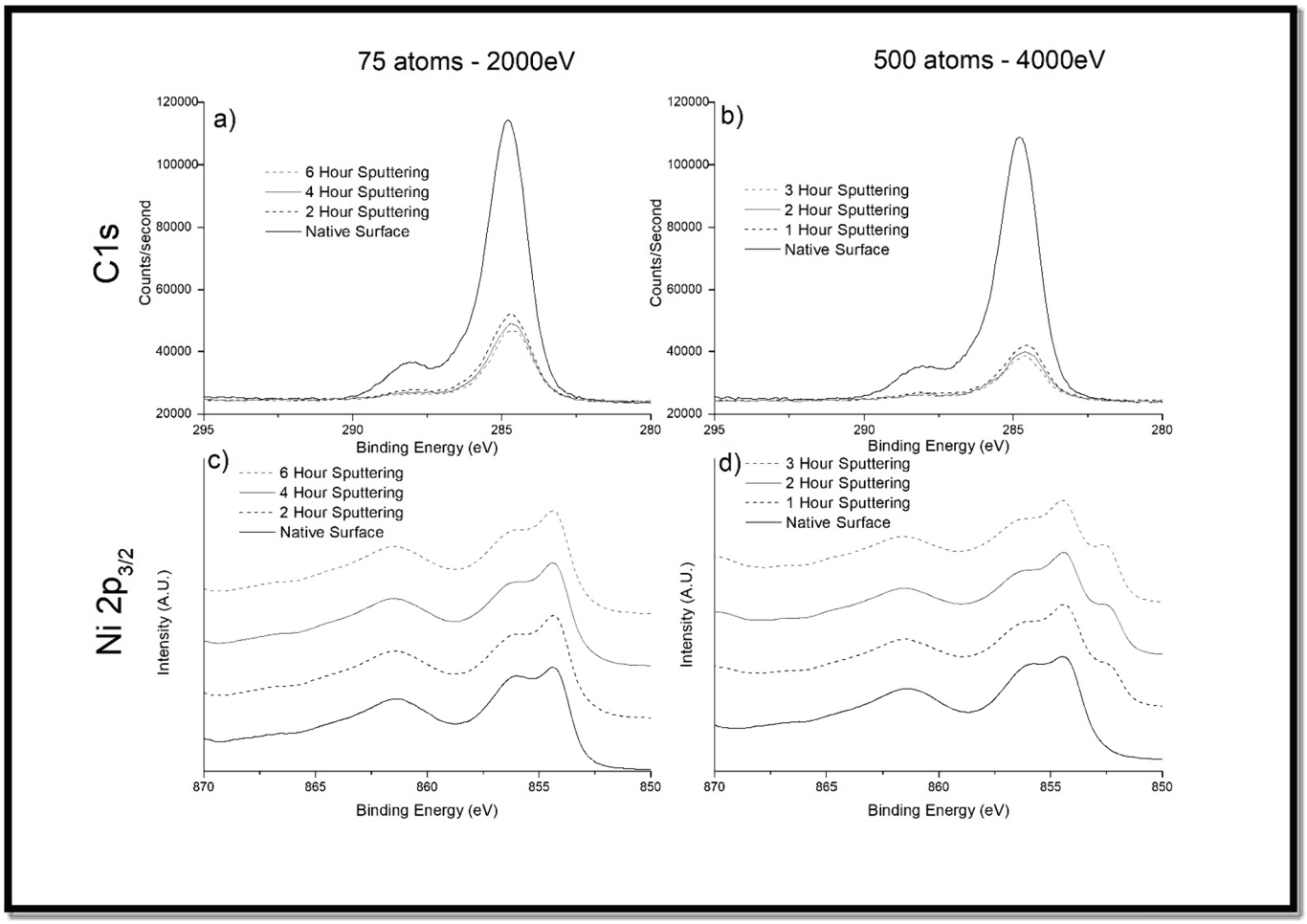

Fig. 7. Spectra recorded for the long-term cluster sputtering tests a) C1s for 75 atom, 2000 eV sputtering b) C1s for 500 atom, 4000 eV sputtering c) Ni2$p_{3/2}$ for 75 atom, 2000 eV sputtering d) Ni2$p_{3/2}$ for 500 atom, 4000 eV sputtering.

sputtering point, while the intermediate, 1000 eV energy sputtering yielded a greater extent of reduction.

Fig. 6b illustrates the metal to oxide ratios that were found when sputtering with the cluster argon ion source. As shown in the figure, significant sputtering reduction occurred with energies of 8000 eV and 4000 eV at cluster sizes of 500 and 75 atoms which correlated with the observed results present in Fig. 4. For both 4000 and 8000 eV ion energies, the metal to oxide area ratios are low when cluster sizes of 2000 atoms are used, suggesting that larger cluster sizes may avoid extensive sputtering reduction. However, this may be attributable to lower sputtering rates associated with lower energy to cluster size ratios. At the lowest cluster ion energy of 2000 eV, the extent of reduction is low as signified by the low metal to oxide ratios, suggesting that lower energy sputtering is desirable to avoid reduction.

3.5. Long term cluster sputtering

Fig. 7 contains the C1s and Ni2$p_{3/2}$ spectra recorded from the oxidized nickel following etching with 4000 eV, 500 atom clusters and 2000 eV, 75 atom clusters for three cycles of one and two hours per cycle, respectively. Notably, the absolute intensity is presented for the C1s spectra. For both cluster parameters, the carbon signal decreased significantly from the native state to the first sputtering level. Subsequent sputtering cycles resulted in a further decrease in the carbon content present, however, the decrease is marginal relative to the initial cycle. Residual carbon may be present due to the textured morphology shown in Fig. 2c. As shown in Fig. 7a and 7b, the higher energy cluster sputtering removed more carbon relative to the 2000 eV cluster sputtering. However, as shown in Fig. 7c and 7d, significant reduction was experienced when 500 atom, 4000 eV clusters were used while the 75 atom, 2000 eV clusters did not result in extensive reduction. It is likely that the low energy clusters are not sputtering the oxide which may explain the lack of observed reduction [22]. While removal of the oxide without reduction is desirable, the ability to remove surface contaminants such as carbon is useful as it allows for greater signal strength to be achieved from the elements of interest. Furthermore, in cases where oxygen speciation is of interest, removal of adventitious carbon may be beneficial as it has recently been estimated that approximately 25 % of the adventitious carbon species are associated with oxygen [24].

4. Conclusion

Sputtering induced reduction of nickel was observed in the Ni 2p X-ray photoelectron spectra for all monatomic sputtering parameters used to sputter oxidized nickel. For cluster source sputtering, reduction was observed when high energy and low cluster size parameters were selected. For the higher energies of 4000 eV and 8000 eV, significant reduction was limited when larger cluster sizes of 2000 atoms were used which may be due to the lower sputtering rate achieved through their use. At the lowest energy of 2000 eV, cluster sputtering resulted in an insignificant amount of metal being produced, regardless of cluster size. Significant reduction was observed at an energy of 4000 eV and cluster size of 500 atoms with an E/n value of 8 eV/atom while a higher E/n value of 26.67 eV/atom for the 2000 eV and 75 atom avoided significant

reduction, suggesting that the extent of reduction caused by cluster ion sputtering does not vary monotonically with E/n value. It is possible that the low energy clusters were not able to sputter the oxidized nickel. Despite this, low energy clusters may minimize the risk of damaging surface species of interest while sputtering to remove unwanted surface contaminants. In future publications, sputtering rates will be determined for cluster sputtering through the use of oxide films of known depths. This will elucidate if the low extent of reduction experienced by low energy cluster sputtering is due to an inability to remove the oxide. Additionally, multiple other oxide systems will need to be explored due to differing propensities for sputtering induced reduction. It is important to note that the observed results may not be easily transferable to non Thermo Scientific systems; however, the observed results may serve as a guideline when performing surface cleaning and encourage all users to explore the use of low energy clusters for sputtering sample surfaces. Future work will explore this phenomenon for samples with different compositions, with the aim to develop a comprehensive model and predictive capability for sputtering induced reduction for a variety of oxide systems.

CRediT authorship contribution statement

Craig Moore: Writing – original draft, Methodology, Investigation, Formal analysis, Data curation, Conceptualization. **Jeremy Moon:** Writing – review & editing, Methodology, Investigation, Formal analysis, Data curation, Conceptualization. **Dev Chidambaram:** Writing – review & editing, Supervision, Resources, Project administration, Methodology, Funding acquisition.

Declaration of competing interest

The authors declare that they have no known competing financial interests or personal relationships that could have appeared to influence the work reported in this paper.

Data availability

Data will be made available on request.

Acknowledgements

The purchase of the X-ray photoelectron spectrometer, housed in the Materials and Electrochemical Research Laboratory, was supported by the National Science Foundation through NSF MRI award 2117820. This work was supported by the Department of Energy (DOE), under contracts DE-AR0001697 (ARPA-e) and NE0008236 (NEUP). Drs. Jenifer Shafer (ARPA-e) and Kenny Osborne (NEUP) serve as program managers for the DOE awards. C.M. is supported by DOE's Nuclear Energy Graduate Fellowship under award DE-NE0009105.

References

[1] D.N.G. Krishna, J. Philip, "Review on surface-characterization applications of X-ray photoelectron spectroscopy (XPS): recent developments and challenges,", Appl. Surf. Sci. Adv. 12 (2022/12/01/ 2022) 100332 https://doi.org/10.1016/j.apsadv.2022.100332.

[2] R. Steinberger, et al., "Chemical degradation of selected zn-based corrosion products induced by C60 cluster, ar cluster and Ar+ ion sputtering in the focus of X-ray photoelectron spectroscopy (XPS),", Appl. Surf. Sci. 403 (2017/05/01/ 2017) 15–22, https://doi.org/10.1016/j.apsusc.2017.01.105 (in en).

[3] A.A. Ellsworth, C.N. Young, W.F. Stickle, A.V. Walker, "New horizons in sputter depth profiling inorganics with giant gas cluster sources: niobium oxide thin films,", Surf. Interface Anal. 49 (10) (2017 2017) 991–999, https://doi.org/10.1002/sia.6259 (in en).

[4] A.R. González-Elipe, G. Munuera, J.P. Espinos, J.M. Sanz, "Compositional changes induced by 3.5 keV Ar+ ion bombardment in ni-ti oxide systems: a comparative study," (in en), Surf. Sci. 220 (2) (1989/10/02/ 1989) 368–380, https://doi.org/10.1016/0039-6028(89)90239-2.

[5] A.R. González-Elipe, R. Alvarez, J.P. Holgado, J.P. Espinos, G. Munuera, J.M. Sanz, An XPS study of the Ar+-induced reduction of Ni2+ in NiO and ni-si oxide systems, Appl. Surf. Sci. 51 (1–2) (1991) 19–26, https://doi.org/10.1016/0169-4332(91)90058-R.

[6] A.R. Gonzalez-Elipe, J.P. Holgado, R. Alvarez, G. Munuera, Use of factor analysis and XPS to study defective nickel oxide, J. Phys. Chem. 96 (7) (1992) 3080–3086, https://doi.org/10.1021/j100186a056.

[7] J.B. Malherbe, S. Hofmann, J.M. Sanz, "Preferential sputtering of oxides: a comparison of model predictions with experimental data,", Appl. Surf. Sci. 27 (3) (1986/12/01/ 1986) 355–365, https://doi.org/10.1016/0169-4332(86)90139-X (in en).

[8] R. Kelly, "On the problem of whether mass or chemical bonding is more important to bombardment-induced compositional changes in alloys and oxides,", Surf. Sci. 100 (1) (1980/10/02/ 1980) 85–107, https://doi.org/10.1016/0039-6028(80)90446-X (in en).

[9] R. Simpson, R.G. White, J.F. Watts, M.A. Baker, "XPS investigation of monatomic and cluster argon ion sputtering of tantalum pentoxide,", Appl. Surf. Sci. 405 (2017/05/31/ 2017) 79–87, https://doi.org/10.1016/j.apsusc.2017.02.006 (in en).

[10] J. D. P. Counsell, A. J. Roberts, W. Boxford, C. Moffitt, and K. Takahashi, "Reduced Preferential Sputtering of TiO₂ using Massive Argon Clusters," J. Surf. Anal. vol. 20, no. 3, pp. 211-215, 2014-01-01 2014, doi: 10.1384/jsa.20.211.

[11] J.T. Moon, E.J. Schindelholz, M.A. Melia, A.B. Kustas, D. Chidambaram, Corrosion of additively manufactured CoCrFeMnNi high entropy alloy in molten NaNO3-KNO3, J. Electrochem. Soc. 167 (8) (2020/05/08 2020) 081509, https://doi.org/10.1149/1945-7111/ab8ddf.

[12] K. O'Neill, Z. Karmiol, J. Groth, H. Alves, D. Chidambaram, Corrosion behavior of high nickel alloys in molten nitrate solar salt, J. Electrochem. Soc. 168 (2) (2021) 021502.

[13] G. Cao, V. Firouzdor, K. Sridharan, M. Anderson, T.R. Allen, Corrosion of austenitic alloys in high temperature supercritical carbon dioxide, Corros. Sci. 60 (2012/07/01/ 2012) 246–255, https://doi.org/10.1016/j.corsci.2012.03.029.

[14] Y. Shi, B. Yang, and P. Liaw, "Corrosion-Resistant High-Entropy Alloys: A Review," Metals, vol. 7, no. 2, p. 43, 2017-02-05 2017, doi: 10.3390/met7020043.

[15] D. Rodriguez, A. Merwin, Z. Karmiol, and D. Chidambaram, "Surface chemistry and corrosion behavior of Inconel 625 and 718 in subcritical, supercritical, and ultrasupercritical water," Appl. Surf. Sci. vol. 404, pp. 443-451, 2017-05-01 2017, doi: 10.1016/j.apsusc.2017.01.119.

[16] A. Merwin, D. Chidambaram, The effect of Li0 on the corrosion of stainless steel alloy 316L exposed to molten LiCl-Li2O-li, Corros. Sci. 126 (2017/09/01/ 2017,) 1–9, https://doi.org/10.1016/j.corsci.2017.04.026.

[17] W. Phillips, D. Chidambaram, Corrosion of stainless steel 316L in molten LiCl-Li2O-li, J. Nucl. Mater. 517 (2019) 241–253.

[18] W. Phillips, D. Chidambaram, Effect of metallic li on the surface chemistry of inconel 625 exposed to molten LiCl-Li2O-li, J. Electrochem. Soc. 166 (11) (2019) C3193.

[19] A.P. Grosvenor, M.C. Biesinger, R.S.C. Smart, N.S. McIntyre, New interpretations of XPS spectra of nickel metal and oxides, Surf. Sci. 600 (9) (2006/05/01/ 2006) 1771–1779, https://doi.org/10.1016/j.susc.2006.01.041.

[20] G. Greczynski, L. Hultman, X-ray photoelectron spectroscopy: towards reliable binding energy referencing, Prog. Mater. Sci. 107 (2020/01/01/ 2020) 100591, https://doi.org/10.1016/j.pmatsci.2019.100591.

[21] M. P. Seah, "Universal Equation for Argon Gas Cluster Sputtering Yields," J. Phys. Chem. C, vol. 117, no. 24, pp. 12622-12632, 2013-06-20 2013, doi: 10.1021/jp402684c.

[22] R. Grilli, R. Simpson, C.F. Mallinson, M.A. Baker, Comparison of Ar+ monoatomic and cluster ion sputtering of Ta2O5 at different ion energies, by XPS: part 2 - cluster ions, Surf. Sci. Spectra 21 (1) (2014) 68–83, https://doi.org/10.1116/11.20140702.

[23] Z. Wang, C. Carrière, A. Seyeux, S. Zanna, D. Mercier, P. Marcus, Thermal stability of surface oxides on nickel alloys (NiCr and NiCrMo) investigated by XPS and ToF-SIMS, Appl. Surf. Sci. 576 (2022/02/01/ 2022) 151836, https://doi.org/10.1016/j.apsusc.2021.151836.

[24] L.H. Grey, H.-Y. Nie, M.C. Biesinger, Defining the nature of adventitious carbon and improving its merit as a charge correction reference for XPS, Appl. Surf. Sci. 653 (2024/04/30/ 2024) 159319, https://doi.org/10.1016/j.apsusc.2024.159319.